Geomechanical modeling of rock fracturing and associated microseismicity

DREW CHORNEY, PIYUSH JAIN, MELANIE GROB, and MIRKO VAN DER BAAN, University of Alberta

Microseismic monitoring is increasingly being used to assess in real time the effectiveness of hydraulic fracture treatments. Operators are interested in three key questions. (1) Where are the microseismic events occurring (what is the size of the microseismic cloud)? (2) What is the failure mechanism (are fractures opening, closing, or shearing)? (3) Why is failure occurring in specific locations but not others (why are fractures not always symmetric with respect to the injection well and what is the geomechanical behavior of the reservoir)? In particular, the last question is difficult to answer from the recorded seismicity alone because the geomechanical behavior depends on the in-situ stress field, the local rock properties (lithologies), and any existing areas of weakness including faults, fractures and joints (Grob and Van der Baan, 2011). Geomechanical modeling can thus play a key role in better understanding both brittle and ductile deformation inside a reservoir because of hydraulic fracturing and the resulting microseismicity.

Bonded-particle modeling (BPM) is becoming an important computational tool for modeling the complex dynamical behavior of rocks rupturing given a set of boundary conditions (Potyondy and Cundall, 2004). Rocks are modeled as the aggregation of (typically) thousands of bonded spherical particles with the goal of reproducing the macroscopic properties of the material and possibly additional features such as microseismicity. This method allows the modeling of realistic materials by specifying appropriate intrinsic particle properties as well as inter-particle (bond) properties. Rupture is modeled through the breaking of the bonds that link the particles (Hazzard et al., 2000). Thus it is only the material properties, primarily the bond strength, which determine the size and shape of a rupture, providing a clear link between the geomechanics occurring in a reservoir and the recorded microseismicity. The resulting source mechanism is inferred from the type of bond breakages (normal or shearing) and their temporal and spatial evolution. A bonded-particle method therefore allows one to investigate in a controlled fashion the interaction of geomechanical reservoir behavior, rock properties, in-situ stress field, existing fractures and the resulting microseismic event locations, source mechanisms, and both seismic (brittle) and aseismic (plastic) deformation.

Here we demonstrate the utility of the method by simulation of triaxial compression tests using calibrated sandstone models. Specifically, the models are tested with and without the introduction of a circular plane of weakness. The kinetic energy in the system is monitored and moment tensors for the failure mechanisms are extracted. The models show fault nucleation in the post peak stress regime for homogeneous samples and localization of bond failures at the edges of the joints for the samples with the circular planes of weakness. The kinetic energy from the bond breakages is compared with the radiated energy, the discrepancy between them being about two orders of magnitude.

Bonded-particle model

A synthetic rock model is formulated by generating a set of particles inside a finite domain, and specifying the contact properties for inter-particle bonds (Potyondy and Cundall, 2004; Figure 1a). Parallel bonds are used to specify the interactions between two particles in contact and are representative of cementation between the two adjacent particles. This "cement" allows both

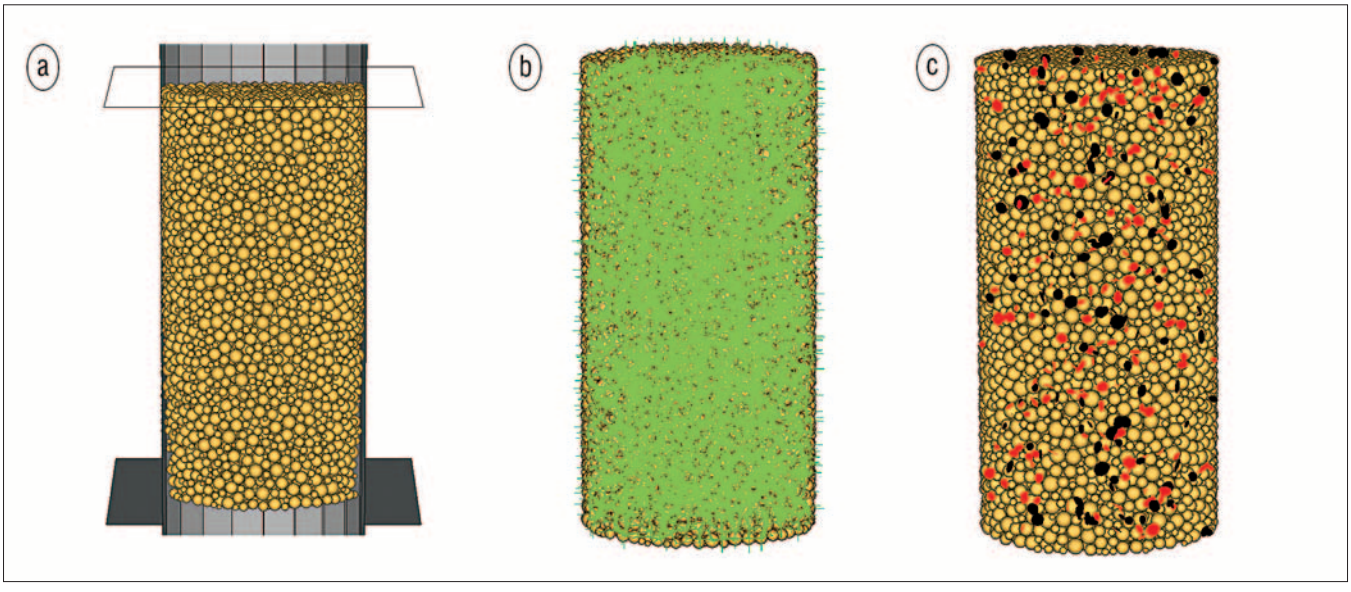

Figure 1. *Images of the calibrated sandstone. (a) The assembly sample showing the confining walls. (b) The force chains between particles shown in green before compression. (c) The bond breakages after stress has been applied to the assembly (normal bond breakages in red and shear bond breakages in black).*

forces and moments to be transmitted over a finite area (either circular or rectangular). The force on each ball (Figure 1b) is linearly proportional to the displacement between the balls (i.e., linear springs). The force can be resolved into normal and shear components, with coefficients of proportionality given by the normal stiffness k_n and shear stiffness k_s, respectively. Parallel bonds allow for both compressive and tensile forces depending on the sign of the contact displacement. The intrinsic ball properties include the density ρ (kg m^{-2}), radius r (m), and friction μ (dimensionless).

This assembly of particles can deform freely and bonds can be broken to represent local failure (Figure 1c). Bonds are characterized by normal and shear strengths and, together with the friction coefficients, are used to model tensile and shear failure. Such a discontinuum-based approach seems more appropriate to model rock deformation through failure since it eliminates the need for complex constitute relations required for continuum approaches (Hazzard et al., 2000).

To simulate the behavior of an interface, BPMs can use a smooth-joint contact model (for an overview, see Ivars et al., 2011). The essential idea is that particles can slide past one another along a plane irrespective of particle size or contact orientation. The smooth joint reduces the effect of the local topography or rugosity intrinsic of a plane composed of spheres.

Finally, with all parameters set, the dynamical evolution of a particle assembly is achieved by the repeated and simultaneous application of both a force-displacement relation and integration of Newton's second law to calculate new particle velocities and positions after a small time increment. For a more thorough discussion of the theory behind the BPM, see Potyondy and Cundall.

An essential first step is model calibration, which is achieved by comparing compression and fracture simulations with known properties of materials measured from equivalent laboratory tests. Here the microparameters of the BPM simulation (i.e., particle and bond properties) are "tuned" until the desired behavior of the assembly is attained.

We simulate a cylindrical sample of sandstone with height 20 mm and radius 5 mm, using a parallel-bonded model. By performing unconfined triaxial tests, the model is calibrated to a Young's modulus, E, of 14.5 GPa, and Poisson's ratio, ν, of 0.30. The unconfined peak stress of the sample, σ_f, is 105 MPa, with a crack initiation stress, σ_{ci}, of 47 MPa. For this model, the crack initiation stress occurs when the number of bond breakages is 5% of the total breakages at peak stress. The following macroscopic properties are obtained using the procedures outlined in Potyondy and Cundall. See Tables 1 and 2 for in-depth parameters of the calibrated sample.

Grains (particles)	Cement (bonds)
$\rho = 3000$ kg/m^3	
$D_{max}/D_{min} = 2.8$	$\bar{\lambda} = 1.0$
$E_c = 16$ GPa	$\bar{E}_c = 16$ GPa
$k_n/k_s = 8.423$	$\bar{k}_n / \bar{k}_s = 8.423$
$\mu = 0.5$	$\bar{\sigma}_c = \bar{\tau}_c = 112 \pm 33$ MPa

Table 1. *PFC^{3D} microproperties for sandstone, where $\bar{\lambda}$ is the parallel bond radius, E_c is the micro Young's modulus of the particles, $\bar{E}_c$ is the micro Young's modulus of the parallel bonds, $\bar{k}_n$ is the normal stiffness of the parallel bond, $\bar{k}_s$ is the shear stiffness of the parallel bond, $\bar{\sigma}_c$ is the normal parallel bond strength, and $\bar{\tau}_c$ is the shear parallel bond strength.*

A general comment is in order regarding the tensile strength of parallel-bonded particle models. It is well documented that, for a bonded sample calibrated to a set of elasticity parameters and compressive strength, the tensile strength of the sample is overestimated (Potyondy, 2011). This is a limitation of the model, which uses spherical as opposed to more realistic granular particles. Grain/clump-based models and flat jointed models attempt to better model both the compressive and tensile strengths of rock samples (Potyondy, 2012). Therefore, in the following simulations the tensile strength of the sample is higher than that of a sandstone, by an estimated 5–6 times. As rocks under compression tend to fail first by tensile fracturing, the samples will be somewhat stronger.

Microseismicity

Bond breakages, and the associated release of strain energy, form seismic events (Hazzard et al., 2000). Specifically, the energy released during bond breakages, in the form of seismic waves, triggers further cracking by increasing local stresses, which exceed the strength of neighboring bonds. The coalescence of these microcracks constitutes a macrorupture.

The moment tensor corresponding to an event can be computed by analyzing the force changes at contacts around the source particles (Hazzard and Young, 2004). The moment tensor is then calculated at each time step over the duration of the event by assuming that a shear fracture propagates at half the shear-wave velocity of the medium (i.e., from the time of breakage to twice the time for a shear wave to propagate to the edge of the source area). If a new crack forms within the source surface of an active crack, the two cracks are considered part of the same seismic event. The source area *S* is expanded to enclose all source particles and the time is reset to zero. This algorithm requires the use of dynamic damping in which damping of the system is reduced when cracking occurs. It is important to note that this causes a relative increase of kinetic energy in the system which may disrupt bonds close to failure. In fact, a sample has been documented to have a ~15% reduction in peak strength with the introduction of dynamic damping (Hazzard et al., 2000). Consequently, this failure tends to be more abrupt yielding stress-strain curves with jagged peaks.

Mechanical observations

Using a calibrated sandstone model, several tests are performed. The first set of simulations are conducted on the intact calibrated sample. Stress-strain curves at 0, 20, and 40 MPa confining pressures are obtained (Figure 2a). The simulations are run until 80% of the absolute peak stress is achieved (post peak stress). As expected, an increase in confining pressure increases both crack initiation and peak stress of the sandstone. In the unconfined triaxial test, the failure is likely a result of tensile failure and the bond breakages in the sample are uniform throughout the

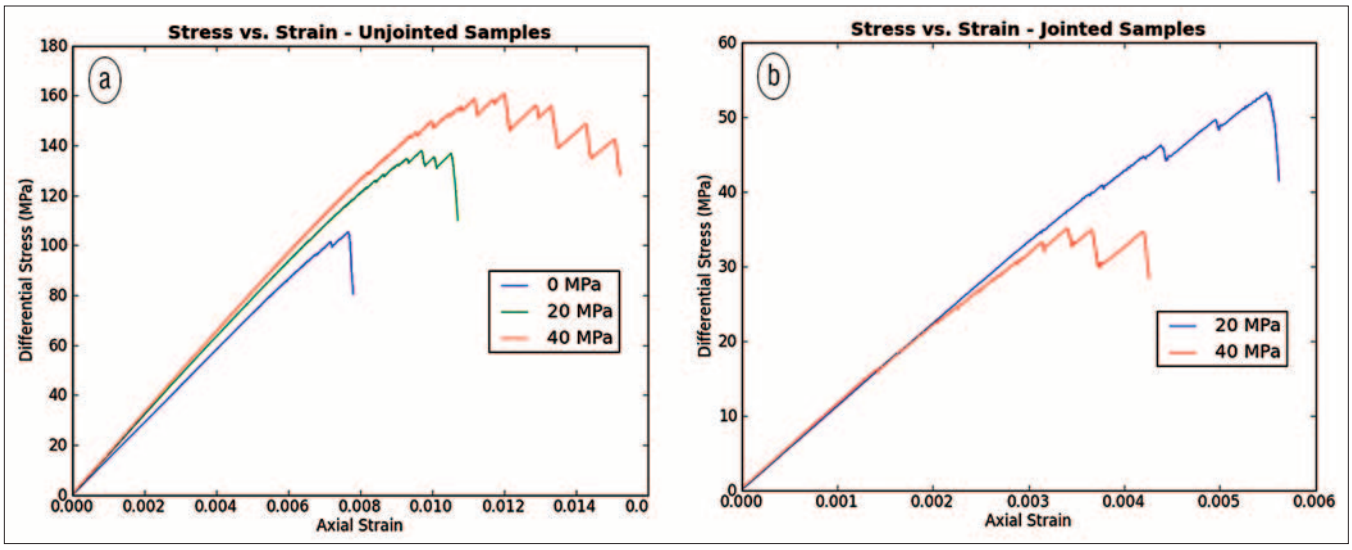

Figure 2. *Differential stress strain curves for (a) homogenous samples and (b) samples with circular smooth joint inserted.*

sample. For the failure of the samples under confinement, shear fracture is readily observed as the bond breakages localize along distinct planes.

The next set of tests uses the same calibrated sandstone model with the introduction of smooth joints. A circular joint is placed at 27° from the vertical axis with a radius of 6 mm (Figure 3). The coefficient of friction of the joint is set at 0.2. Triaxial tests are conducted at confining pressures of 20 and 40 MPa. Figure 2b shows the corresponding stress-strain curves. Comparing the jointed and nonjointed samples at 20 MPa confinement, the peak differential stress is reduced from 137.8 to 53.2 MPa. In general, the strength of the sample is dramatically reduced by the introduction of the joint. New cracks are mainly located at the edges of the joints as propagation of the plane of weakness becomes the primary mechanism for fracture development (Figure 3b). Further analysis shows that increasing the confining pressure substantially decreases the differential peak strength of the jointed sample (Figure 2b). This appears counterintuitive as it is expected that the sample will be strengthened with increased confining stress. However, in the present case, the size of the asperity is large in relation to the size of the sample. The edges of the crack are close to the radial boundary. This induces a significant near-stress field in the proximity of the crack tips contrary to far-stress fields usually considered in rock mechanics (Jaeger et al., 2001). In the axial direction, the source of the stress field is further out from the joint. The result is that the sample is weakened despite the increase in confining stress. We have found that simulations with smaller joint lengths (relative to specimen size) reproduce the familiar increase in peak strength with increasing confinement pressure (Table 3).

The energy released by the failure of bonds in the samples can be computed from the spikes in kinetic energy following bond breakages. The kinetic energy of the sample is computed by measuring the instantaneous velocities (both translational and rotational) of all particles in the system, both before and after bond breakages. The kinetic energy before failure is subtracted from the maximum of the kinetic energy spike following a breakage, and the total kinetic energy emitted is then estimated from the sum over all bond breakages.

Property	PFC^{3D}
E (GPA)	14.5
υ	0.30
σ_f	105
σ_{ci}	47
ρ (kg/m^3)	1920

Table 2. *Macroproperties from uniaxial tests.*

Routines are also available to calculate the boundary work at any given time, which gives the total input energy of the system. Measuring the ratio of the bond failure kinetic energy and the system input energy gives an estimated percentage for the brittle failure of the simulation (Table 4). For the sample with 0 MPa confinement, the kinetic energy from brittle failure is about 9% of the input energy. A key observation is that brittle failure is reduced approximately by half in the presence of confining pressure. This result is supported by laboratory experiments that show a higher mean stress will cause failure to be more ductile than brittle. With the introduction of joints, the change in brittle energy content is not significant. This may be a symptom of the timescale of the simulations, which are run until 80% peak failure is met. Instead, it may be more suitable to have the simulation end when a fixed axial strain is met or to hold the energy input of the system constant across all simulations.

Microseismicity analysis

The number of microseismic events in each simulation follows an exponential curve as the applied stress increases. This behavior is similar to real laboratory experiments (Jouniaux et al., 2001). A comparison of the total number of events for samples without a joint (Table 5) shows that a higher confinement leads to more failure. For simulations with the joint, the plane of weakness accommodates the deformation and thus reduces the peak strength of the specimen. The number of events is

drastically reduced. By construction, the joint will also decrease the number of bond breakages as particles neighboring the joint are not bonded. These results are consistent with laboratory experiments performed by Jouniaux et al.

The analysis of the microcracks shows that more than two thirds of the events are single bond breakages (Table 5). A single bond event has an average magnitude of −7.7 although the magnitude can range between −9 to −7 depending on the force variations. The radiated energy calculation, E_s, is based on the Gutenberg-Richter relationship between the moment magnitude M_W and the energy (Kanamori, 1977):

$$E_s = 10^{(11.8 + 1.5 \times M_W)} \quad (1)$$

The ratio between the radiated energy and the boundary work is below 0.1%. E_S is also compared with the measured kinetic energy after the bond breakages in the sample. The discrepancy between the two is more than two orders of magnitude. However, it should be noted that the Gutenberg-Richter formula was developed for earthquakes with a magnitude higher than 5 and should certainly be modified for smaller-scale types of events. Additionally, this empirical relationship assumes a double-couple type of mechanism whereas most of the events in our simulation show tensile behavior (Figure 5).

A sparse distribution of events is displayed in Figure 4 for the unconfined experiment at the three different stages. A macro fracture plane appears after the peak stress has been reached for the nonjointed sample at 40 MPa confinement. For the jointed samples, the plane of weakness causes the events to localize near the smooth joint early on in the simulations. Differences in event location distributions are quantified through the fractal dimension D, which measures the clustering of events (Grassberger and Procaccia, 1984). A D value close to 3 signifies a uniformly distributed cloud of events whereas a D value below 2 is found for events located over a planar structure. A D value above 2.7 is found over all events for all simulations without the joint (cf Table 5). This is in agreement with the visual spread of the events observed. A D value around or below 2 is found for the jointed experiments at confining pressures 20 and 40 MPa. This suggests that events localize along planar structures in the sample.

Another important statistical value is the exponent of the power law distribution of the event magnitudes first described by Gutenberg and Richter (1944), denoted by b. A low b-value implies more large events whereas a high b-value means more small events. In our simulations, the lowest b-values are found for the 40 MPa confined experiments, which are consistent with Amitrano (2003) who shows b-values depend inversely on stress. More recently, b-values over 2 have been found to be directly related to tensile fracture mechanisms (Maxwell et al., 2008). The b-values computed for all simulations are rather high, typically above 2. The source mechanisms for events are represented on a Hudson plot (Hudson et al., 1989) in Figure 5. They predominantly range from opening to closing types of events, so tensile failure seems to be indeed correlated with high b-values. A few events are at the center of the Hudson plot,

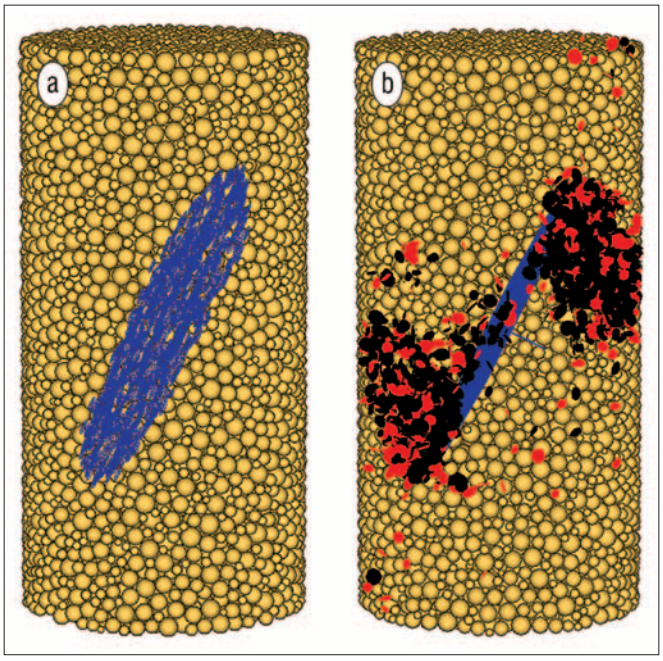

Figure 3. *The calibrated sandstone sample with circular smooth joint inserted. The joint is 27° off the vertical axis and has a radius of 6 mm. (a) Sample before simulations. (b) 40-MPa sample after triaxial test (normal bond breakages in red and shear bond breakages in black).*

Confinement pressure	No joint	Joint 6 mm	Joint 4 mm	Joint 3 mm	Joint 2 mm
20 MPa	157.8 MPa	73.75 MPa	129.8 MPa	145.7 MPa	154.7 MPa
40 MPa	200.5 MPa	75.3 MPa	149.3 MPa	171.1 MPa	192.2 MPa

Table 3. *Absolute peak stress of the samples. Sample radius is 5 mm. Table lengths are radii of the circular joints.*

Experiment	Kinectic energy from bond breakages (J)	Boundary work (J)	Brittle failure percentage
0 MPa–No joint	0.0698	0.7095	9.84 %
20 MPa–No joint	0.0761	1.7287	4.40 %
40 MPa–No joint	0.1745	3.4986	4.99 %
20 MPa–Jointed	0.0194	0.4449	4.36 %
40 MPa–Jointed	0.0225	0.4156	5.41 %

Table 4. *Energy content at the end of simulations.*

which indicates a strike-slip type of mechanism. No difference in terms of source mechanism can be found between the different stages of the experiment. Longer simulations are expected to expose a complete localization of the events along a macro fracture plane. In this case, sliding will occur (Jouniaux et al.), leading to more strike-slip type of mechanisms.

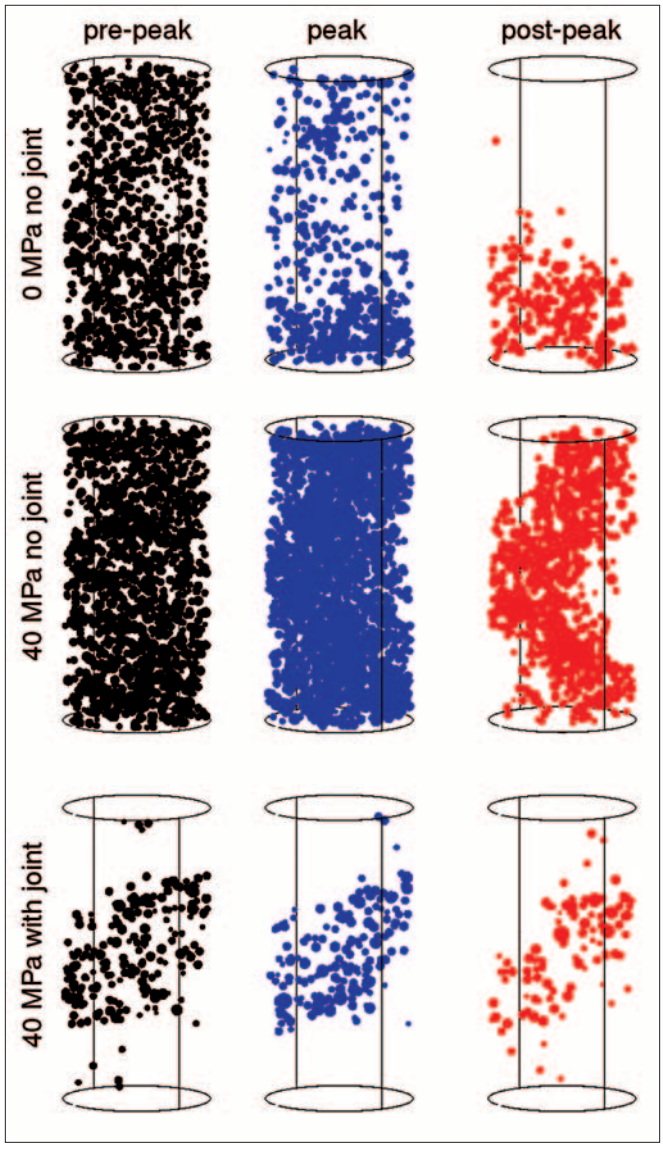

Figure 4. *Images of the event locations at different stages for three different simulations.*

Discussion

In this article, we simulate acoustic emissions and geomechanical deformation in a simple triaxial compression test to demonstrate the capabilities of bonded-particle methods. Obviously the actual geomechanical behavior inside and surrounding a reservoir during hydraulic fracturing is significantly more complex; yet analysis of the energy balance already allows us to draw some conclusions on ratios between aseismic (ductile) versus seismic (brittle) deformations.

Often substantial differences are estimated between the total input energy inferred from fluid injection rates and pressures, the fracture energy to pry apart the walls of a single large fracture, and the radiated energy observed from recorded seismicity. The injected energy is 10^4–10^7 times larger than the estimated radiated seismic energy, and the fracture energy is inferred to equal 15–40% of the input energy (Maxwell et al., 2008; Boroumand and Eaton, 2012).

These energy calculations incorporate several key factors and assumptions. The injected energy includes the work done to cause local rock failure and deformation but also fluid friction inside the well, rocks, and any leak off. The fracture energy purely entails tensile opening of an existing crack but excludes the work required to create new fractures. Estimates of the amount of radiated seismic energy are based on empirical laws commonly used in global seismology that assume double-couple source mechanisms and thus pure shear but no tensile deformation (failure).

In geomechanical modeling the boundary work (input energy) equals the sum of exerted body forces (gravity), kinetic energy (bond breakages), frictional work, strain energy (ductile deformation), and internal damping. The kinematic energy includes thus both shear and tensile failure, and represents about 4–10% of the total energy (Table 4). On the other hand, the estimates for the seismic radiated energy comprise only 0.08–0.10% of the total energy (Table 5), and are thus 50–100 times smaller here than the actual amount of brittle failure (work). This implies that computations based on the amount of radiated energy inferred from seismic moment calculations may always significantly underestimate the percentage of incurred brittle failure, partially because the underlying empirical laws exclude tensile failure.

Finally, when examining the radiated or kinetic energy from brittle failure, in either case, the energy is substantially lower than the input energy. It seems reasonable to conclude that ductile deformation must be a significant term in the energy budget for both the proceeding simulations and for hydraulic fracturing experiments in general.

Samples	Number of events	% of single-bond event	Radiated energy	% radiated energy/ boundary work	*b*-value	*D*-value
0 MPa no joint	1723	73	0.000785	0.1	2.35 ± 0.2	2.73 ± 0.11
20 MPa no joint	2868	66	0.001433	0.08	2.25 ± 0.08	2.79 ± 0.08
40 MPa no joint	4276	65	0.002699	0.08	2.14 ± 0.09	2.80 ± 0.09
20 MPa jointed	600	71	0.000282	0.06	2.33 ± 0.13	1.67 ± 0.09
40 MPa jointed	610	73	0.000399	0.08	1.59 ± 0.09	1.54 ± 0.12

Table 5. *Microseismicity analysis.*

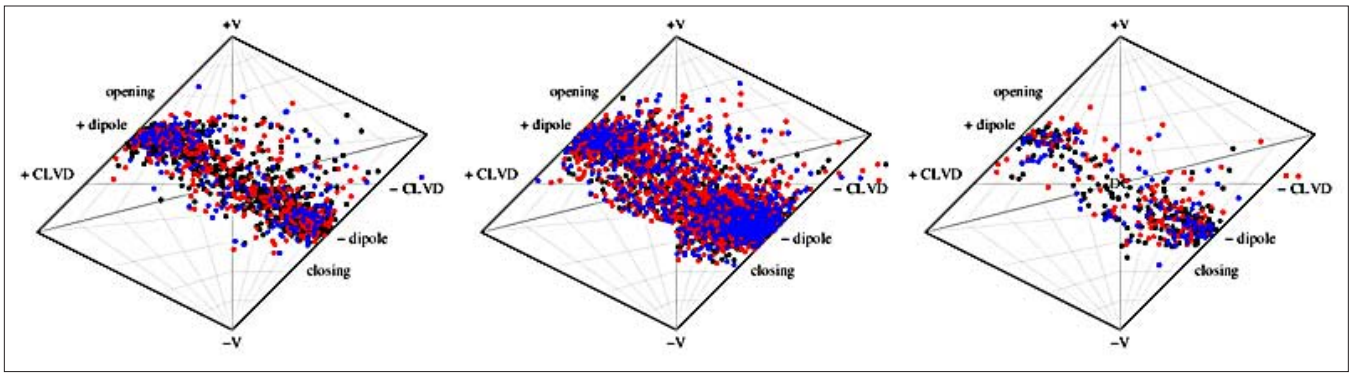

Figure 5. *Source mechanisms of events for the simulations shown in Figure 4 represented on a Hudson plot. The colors define the different stages during the experiments according to Figure 4. 0 Mpa no joint (left), 40 MPa no joint (middle), and 40 MPa with smooth joint (right).*

Conclusion

An important question in the monitoring of a reservoir is what the exact link is between the recorded microseismicity and the actual geomechanics. Independent observations of event locations, source mechanisms and stresses are used to infer their relationship but often observations are not made at the same location (around wells for stresses, further away and deeper for microseismic events) or at the same scale. It is also possible aseismic deformation may take place, preventing the use of recorded microseismicity for deduction of the geomechanical behavior in the reservoir.

One possible way to define the interaction between rupture mechanisms and recorded events is by the use of modeling. In this article, we have used the bonded-particle method to explore the rupture mechanisms of a sandstone model under differing confinement pressures both with and without a joint. We find the radiated energy to be about 50–100 times smaller than the kinetic energy from brittle failure. This suggests the possibility that radiated energy calculated by the Gutenberg-Richter relationship may underestimate the energy incurred from brittle failure. Whatever the case, energy from brittle failure is substantially lower than the input energy suggesting ductile deformation is a significant term in the energy budget. These preliminary experiments produce both interesting and quantifiable results suggesting the bonded particle method is a viable approach for modeling more complicated scenarios. Ultimately, it is both a real desire, and perhaps a possibility, to include the complexity of fluid injection in the hopes of better modeling hydraulic fracturing experiments. TLE

References

Amitrano, D., 2003, Brittle-ductile transition and associated seismicity: Experimental and numerical studies and relationship with the b-value: Journal of Geophysical Research, **108**, B1, 2044, http://dx.doi.org/10.1029/2001JB000680. PubMed

Boroumand, N. and D. W. Eaton, 2012, Comparing energy calculations—hydraulic fracturing and microseismic monitoring: GeoConvention 2012.

Grassberger, P. and I. Procaccia, 1984, Dimensions and entropies of strange attractors from a fluctuating dynamics approach: Physica D. Nonlinear Phenomena, **13**, no. 1–2, 34–54, http://dx.doi.org/10.1016/0167-2789(84)90269-0.

Grob, M., and M. Van der Baan, 2011, Inferring in-situ stress changes by statistical analysis of microseismic event characteristics: The Leading Edge, **30**, no. 11, 1296–1301, http://dx.doi.org/10.1190/1.3663403.

Gutenberg, B. and C. F. Richter, 1944, Frequency of earthquakes in california: Bulletin of the Seismological Society of America, **34**, 185–188.

Hazzard, J. F. and R. Young, 2004, Numerical investigation of induced cracking and seismic velocity changes in brittle rock: Geophysical Research Letters, **31**, no. 1, L01604, http://dx.doi.org/10.1029/2003GL019190.

Hazzard, J. F., R. P. Young, and S. C. Maxwell, 2000, Micromechanical modeling of cracking and failure in brittle rocks: Journal of Geophysical Research, doi:101029/2000JB900085.

Hudson, J. A., R. G. Pearce, and R. M. Rogers, 1989, Source type plot for inversion of the moment tensor: Journal of Geophysical Research, **94**, no. B1, 765–774, http://dx.doi.org/10.1029/JB094iB01p00765.

Jaeger, J. C., N. G. W. Cook, and R. W. Zimmerman, 2007, Fundamentals of rock mechanics (fourth edition): Blackwell.

Jouniaux, L., K. Masuda, X. Lei, O. Nishizawa, K. Kusunose, L. Liu, and W. Ma, 2001, Comparison of the microfracture localization in granite between fracturation and slip of a preexisting macroscopic healed joint by acoustic emissions measurements: Journal of Geophysical Research, **106**, no. B5, 8687–8698, http://dx.doi.org/10.1029/2000JB900411.

Kanamori, H., 1977, The energy release in great earthquakes: Journal of Geophysical Research, **82**, no. 20, 2981–2987, http://dx.doi.org/10.1029/JB082i020p02981.

Maxwell, S.C., J. Shemata, E. Campbell, and D. Quirk, 2008, Microseismic deformation rate monitoring: SPE paper 116596.

Potyondy, D. O. and P. A. Cundall, 2004, A bonded-particle model for rock: International Journal of Rock Mechanics and Mining Sciences, **41**, no. 8, 1329–1364, http://dx.doi.org/10.1016/j.ijrmms.2004.09.011.

Potyondy, D. O., 2011, Parallel-bond refinements to match macroproperties of hard rock, in D. Sainsbury, R. Hart, C. Detournay, and M. Nelson, eds., Continuum and distinct element modeling in Geomechanics (Proceedings, 2nd Internationl FLAC/DEM Symposium): Itasca International, paper 08–04.

Potyondy, D.O., 2012, A flat-jointed bonded-particle material for hard rock: American Rock Mechanics Association, 12–501.

Acknowledgments: This work was supported by the Microseismic Industry Consortium. The authors thank Itasca for providing licenses for the PFC software.

Corresponding author: drchorne@ualberta.ca